THE JOURNAL OF PHYSICAL CHEMISTRY B

ARTICLE

pubs.acs.org/JPCB

Self-Assembly Process of Peptide Amphiphile Worm-Like Micelles

Tomoko Shimada,*[,†] Naoki Sakamoto,[†] Ryuhei Motokawa,[‡] Satoshi Koizumi,[‡] and Matthew Tirrell[§]

[†]New Business Development, Asahi-Kasei Corporation, Jinbocho, Tokyo, Japan

[‡]Japan Atomic Energy Agency, Tokai, Ibaraki, Japan

[§]Institute for Molecular Engineering, University of Chicago, Chicago, Illinois 60637, United States

ABSTRACT: Peptide amphiphile molecules (PA) are remarkably versatile and useful as building blocks for construction of complex supramolecular structures in a bottom-up fashion. Worm-like micelles of PA have been demonstrated to have successful application to creation of synthetic extracellular matrix materials for tissue engineering and regenerative medicine. However, the pathway of the self-assembly process of the PA worm-like micelle has not been fully characterized or understood. This work analyzes the self-assembly process leading to worm-like micelle formation in our designed PA with small-angle neutron scattering and atomic force microscopy. The experimental results demonstrate the existence of transient spherical micelles in the early stage of the process and subsequent micelle chain elongation by attachment of spherical micelles to the end of growing cylindrical micelles to form worm-like micelles in a process mimicking chain-growth polymerization.

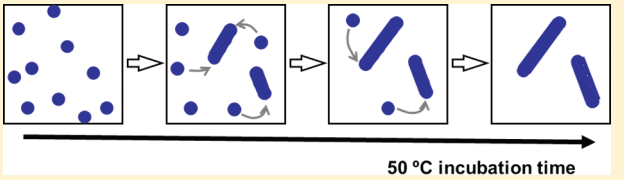

INTRODUCTION

Peptide amphiphiles (PA) are promising as molecular building blocks that can construct complex supramolecular structures in a bottom-up, modular fashion employing the wide variety of molecular designs and bioactivities that can be built into the peptide region. PA comprising hydrophilic peptides and hydrophobic alkyl tails in one molecule form various self-assembled structures, such as spherical micelles, worm-like micelles, bilayer membranes, and vesicles, in a similar fashion to traditional amphiphilic molecules (such as surfactants), depending on the volume and length of the alkyl tail and surface area of the peptide headgroup.[1] These self-assembled structures are useful as carriers and matrices because they can encapsulate and solubilize small hydrophobic molecules and form 3D networks.[2−4] Of the various PA assembly structures the "worm-like micelle" is one of the most attractive structures for application of a functionalized artificial extracellular matrix (ECM) because the diameter of the micelle can be controlled on the nanoscale and bioactivity can be displayed on the micelle surface.[5−10] For example, it has been reported that PA worm-like micelles displaying the isoleucine-lysine-valine-alanine-valine (IKVAV) domain have capacity for directing neural cell differentiation.[7] Knowledge and technology for controlling the nano- and microstructures of the PA assembly to give specific bioactivity of worm-like micelle are very much needed in tissue regenerative therapies. This need for understanding and ability to manipulate the formation process, not only to reach the desired final *structural* state but also to achieve desired *processability* characteristics, such as injectability and subsequent gelation, motivates this work.

In recent years, PA that can form worm-like micelles in certain environments (pH, solvent, concentration, etc.) have been developed, and the presence of β-sheet structure is observed as a common structure in these PA.[11−14] Therefore, β-sheet formation in PA is presumed to play a key role in worm-like micelle formation. However, the studies that actually track the self-assembly processes of PA worm-like micelles are few, and the mechanism of formation is not fully understood. In this work, we study the assembly process into worm-like micelles of the peptide amphiphile (C16-W3K), which has already been reported to form worm-like micelle simultaneously with β-sheet formation in the peptide W3K in our previous study.[15] The useful features of the C16-W3K for this study are simple structure, slow formation speed, and absence of a need for a specific trigger to induce the structural change. The sample was incubated at temperatures approaching 50 °C to adjust the transition time to an adequate range for convenient analytical measurement. The self-assembly structures in the samples at different incubation time are analyzed with small-angle neutron scattering (SANS) and atomic force microscopy (AFM).

EXPERIMENTAL METHODS

Design and Synthesis of the Peptide Amphiphile C16-W3K. The peptide amphiphile C16-W3K (Figure 1) was synthesized by covalent linkage of a peptide W3K and an alkyl tail of C16 (i.e., containing 16 CH_2) using Fmoc solid-phase peptide synthetic methods.[16] The 17-residue peptide (W3K) has been designed[17] to contain 13 alanines to possess high α-helical propensity. Three lysines are incorporated into the peptides for introducing water solubility, presenting angular and longitudinal symmetry around the α-helix axis. Samples for analytical measurements (SANS and AFM) were prepared by adding buffer (10 mM sodium chloride and 1 mM sodium phosphate)

Received: September 21, 2011
Revised: November 29, 2011
Published: December 02, 2011

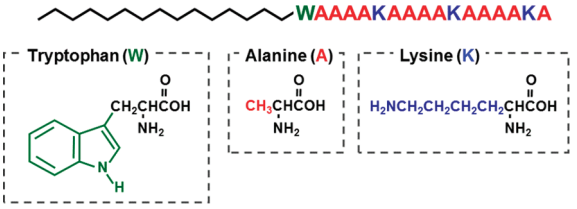

Figure 1. Chemical structure of the peptide amphiphile C16-W3K.

to the C16-W3K at room temperature at a concentration of 0.1 wt % followed by 50 °C incubation.

SANS Measurements. The structural change of the micelle was studied by SANS with SANS-J-II[18−20] at the Japan Atomic Energy Agency, JAEA, in Tokai. Time-resolved SANS measurements were performed by the *T*-jump method as follows: (1) the sample solution was set in the quartz cell with a thickness of 10 mm at room temperature; (2) the sample cell was put into the heater block set on the optical path of the incident neutron beam and regulated at 44.8 °C; (3) the time-resolved SANS measurements were started when the sample was transferred into the heater block. The wavelength λ of the incident beam is 0.5 nm, the camera length was 2.5 m, and the accumulation time of each shot was 10 min. The two-dimensional SANS patterns obtained were averaged circularly and corrected for absorption, the scattering from the empty cell, and the absolute intensity.

AFM Measurements. For AFM analysis, the samples were deposited on freshly cleaved mica and kept for 10 s at room temperature before blowing off any possible small debris on the surface. Experiments were carried out with D3000 (Digital Instruments, Ltd.) in tapping mode. A 50 °C incubation was performed by keeping the sample in a 50 °C water bath for 10, 20, 30, 60, 120, and 210 min.

RESULTS AND DISCUSSION

The structure of our peptide amphiphile C16-W3K is shown in Figure 1. Time-resolved SANS was used to analyze the self-assembly process of the C16-W3K in order to obtain in situ and continuous information.[21] Figure 2 shows the scattered intensity $I(q)$ before and after the T jump from room temperature to 44.8 °C, plotted double logarithmically as a function of the magnitude of the scattering vector q, defined by

$$q = 4\pi \sin(\theta/2)/\lambda \quad (1)$$

where θ is the scattering angle. The SANS profile of the sample before the T jump (Figure 2, open diamonds) shows that the scattering profile is proportional to q^{-4} in the region larger than 0.7 nm^{-1} and to q^0 in the region smaller than 0.3 nm^{-1}, indicating spherical micelles. Though we deduced previously[15] that C16-W3K form spherical micelles in the early stages of self-assembly from the cryo-TEM images, it was difficult to observe the spherical shape clearly due to its kinetic instability and smaller size relative to those of cylindrical shape. The SANS profile is direct experimental evidence for the existence of the spherical micelle as an intermediate preceding worm-like micelle formation. We conjecture that this pathway via the intermediate spherical state is a key factor for forming water-soluble worm-like micelle rather than insoluble aggregates.

In contrast, the profile of the sample after 600 min (Figure 2, filled circles) is also proportional to q^{-4} in the large q region, but the profile is proportional to q^{-1} for small q, indicating a locally

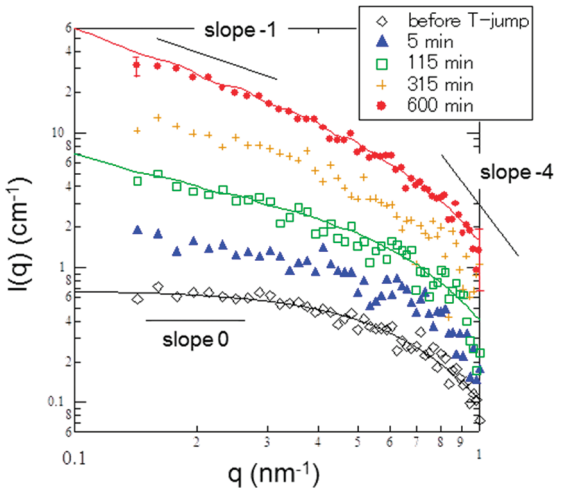

Figure 2. Time-resolved SANS profiles before and after T jump from room temperature to 44.8 °C. Symbols are measured SANS profiles, and solid lines are theoretical scattering curves of spherical and/or cylindrical micelles. To avoid overlaps, the profiles are shifted up with a factor of 2.

cylindrical form of the scatterers, that is, worm-like micelles. Taken together this set of results means that the structure of the micelles changes from spherical to worm-like during incubation.

Black and red lines in Figure 2 show the fitting results of the SANS profiles in samples before and 600 min after the T jump, respectively, to the theoretical scattering equations of sphere (eq 2) and random oriented cylinder (eq 3), respectively.

Sphere

$$I(q) = CN \int_0^\infty P(r) \left[\frac{4\pi r^3}{3} F_{\mathrm{sph}}(qr) \right]^2 \mathrm{d}r \quad (2)$$

$$F_{\mathrm{sph}}(qr) = \frac{3}{(qr)^3}[\sin(qr) - (qr)\cos(qr)]$$

Randomly oriented cylinder

$$I(q) = \frac{CN}{2} \int_0^\infty \mathrm{d}r \int_0^\pi \mathrm{d}\beta P(r)[\pi r^2 l F_{\mathrm{cyl}}(\beta, q, r, l)]^2 \sin\beta \quad (3)$$

$$F_{\mathrm{cyl}}(\beta, q, r, l) = \frac{2 \sin\left(\frac{ql}{2}\cos\beta\right)}{\frac{ql}{2}\cos\beta} \frac{J_1(qr\sin\beta)}{qr\sin\beta}$$

where r is the radius, l is the length of a cylinder, C is a constant independent of q and r, and N is the total number of particles. $P(r)$ is a normalized distribution function describing a number of particles having radius r. We assume that $P(r)$ has the Schultz−Zimm distristribution defined by

$$P(r) = \frac{M^M}{\Gamma(M) r_0^M} r^{M-1} \exp\left(-\frac{M}{r_0} r\right) \quad (4)$$

where M is the shape factor of the distribution, r_0 is the number average of r, and $\Gamma(x)$ is the gamma function. These results exhibit that the SANS profiles before and 600 min after the T jump are well fitted by the theoretical scattering equations of sphere and cylinder, respectively. The parameters obtained from the fittings are shown in Table 1. σ/d_0 is the normalized standard

dx.doi.org/10.1021/jp209105z |J. Phys. Chem. B 2012, 116, 240–243

Table 1. Parameters Obtained from the Fitting of the Profiles by eqs 2 and 3

	before T jump	600 min after T jump
micellar type	spherical	cylindrical
diameter d_0 (nm)	4.9	4.0
σ/d_0	0.32	0.22
cylinder length l (nm)		>20

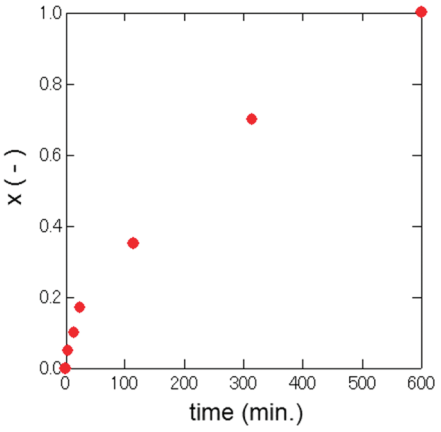

Figure 3. Cylindrical micelle evolution in the samples as a function of incubation time. Vertical axis is the fraction of cylindrical micelles in the self-assembling mixture.

deviation of a diameter, calculated by $\sigma/d_0 = M^{-0.5}$. In the fitting by eq 3 the value of l was set to infinity. Since it can be shown that scattering from a cylinder longer than 20 nm is equivalent in this q range, the length of the cylindrical micelle after 600 min is longer than 20 nm, but a quantitative estimate of the micelle length cannot be obtained from fitting these data.

The scattering profiles of the samples during incubation (5, 115, and 315 min) show that the curves transform between the spherical one (before T jump) and the cylindrical one (after 600 min incubation) gradually over the incubation time. As shown above, elongation of the cylindrical micelle longer than 20 nm makes no difference in this q range. This means that the profile change over incubation time does not derive from elongation of the cylindrical micelle; after that all the spherical micelles have combined into short cylinders at an early stage, since this would result in an abrupt, early transformation of the characteristic scattering from spherical to worm-like. In other words, these profiles should be interpreted as compound curves of the spherical micelles and the cylindrical micelles; the variation of the profile over time indicates the evolution of the sphere/cylinder micelle ratio in the samples.

Therefore, the profile of the sample 115 min after T jump (Figure 2, green line) was fitted by the theoretical compound equation (eq 5) of spherical and cylindrical scattering equations.

$$I(q) = (1 - x)I_{sph}(q) + xI_{cyl}(q) \quad (5)$$

In eq 5, $I_{sph}(q)$ and $I_{cyl}(q)$ are theoretical scattering forms of sphere and cylinder with the parameters shown in Table 1. The profile of the 115 min incubation sample can be well fitted by eq 5, the compound equation of $I_{sph}(q)$ and $I_{cyl}(q)$ (Figure 2, green solid line).

Scheme 1. Self-Assembly Process of Worm-Like Micelle in the Peptide Amphiphile C16-W3K During the 50 °C Incubation

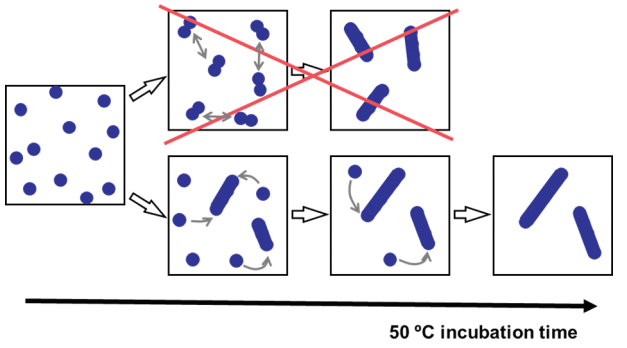

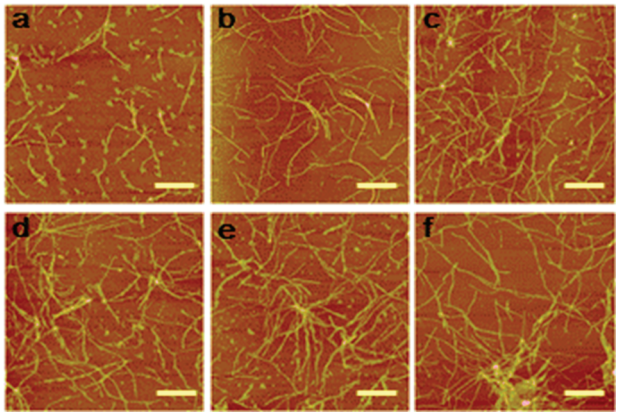

Figure 4. AFM images of dried C16-W3K solution on fleshly cleaved mica after 50 °C incubation of (a) 10, (b) 20, (c) 30, (d) 60, (e) 120, and (f) 210 min (scale bar, 1 μm).

Figure 3 shows the time change of the cylindrical micelle ratio (x) calculated by profile fitting of eq 5. In the fitting, all parameters of $I_{sph}(q)$ and $I_{cyl}(q)$, including the polydispersity parameter, were fixed as the values in Table 1. The data reveal that the ratio of the cylindrical micelle in the sample increases gradually with incubation time and the spherical micelles remain even after a long incubation time (315 min). The remaining spherical micelle and gradual decrease of the spherical micelle may indicate that worm-like micelle formation proceeded by attachment of the sphere to the end of the short cylinder one by one (Scheme 1, lower image), not by simultaneous sphere combining followed by combining between cylinder and cylinder (Scheme 1, upper image). In our previous work, the circular dichroism (CD) measurement of the C16-W3K solution showed the gradual transition of the peptide secondary structure from α-helix and random coil to β-sheet in the C16-W3K during the 50 °C incubation.[15] We believe that the reduction of the effective area of the hydrophilic headgroup in the packing parameter,[1] generally used to predict micelle shapes, due to the secondary structural change, specifically due to attractive hydrogen bonding in the β-sheet, induces the micelle transition from sphere to worm-like.

This interpretation of the trajectory of the assembly process of C16-W3K is also supported by AFM results (Figure 4). AFM images were measured to examine the self-assembly structures

visually in the samples of 10, 20, 30, 60, 120, and 210 min incubation at 50 °C. Though it should be noted the that possibility that the assembly structures observed in AFM images could be different from the state in aqueous media for the SANS experiments because of its dried condition for the AFM measurement, we believe that the AFM images do reflect the assembly structure in aqueous media because the assembly structure is stabilized by the intermolecular hydrogen bonds in the β-sheet. Stabilization of the β-sheet in the dried state was confirmed by IR measurement in the dried samples (data not shown).

All AFM images here show fibril-like materials, i.e., worm-like micelles, while many block-like materials are observed in the sample of 10 min incubation. The block-like material in Figure 4a is presumed to be an aggregate of unstable spherical micelles that have no intermolecular hydrogen bond (CD and IR shows little β-sheet in this sample) during the process of drying. The image of the sample before incubation exhibits just block-like materials, no fibril-like structure (data not shown).

The AFM images exhibit that the length of the worm-like micelles varies greatly in each sample. Even in the 210 min incubation sample we can see some short fibrils. It is also found that the number of the fibrils increases and the longest micelle length in each sample elongates with passage of the incubation time. While the longest worm-like micelle is around 2 μm in 10 min, it becomes about 3 μm at 30 min. At 210 min, the longest fibrils are more than 5 μm in length and more and bigger entangles are also observed.

From these results, we deduce that nucleation of elongated micelles and chain elongation of the micelles occur simultaneously during the assembly process, consistent with both the SANA and the AFM observations.

CONCLUSIONS

In the present paper, we studied the worm-like micelle formation process of the peptide amphiphile C16-W3K with small-angle neutron scattering and atomic force microscopy. The SANS and AFM results showed that the transient spherical micelles exist in the early stage of the process, and subsequently, the micelle chain elongates by attachment of spherical micelles to the ends of growing cylindrical micelles in the elongated micelle formation. The understanding of the process for PA worm-like micelle formation could potentially lead to further applications of PA self-assembling materials. The trajectory we observed here has significant implications, for example, for the rheology of the self-assembling mixture, which could, in turn, affect the utility of these materials in regenerative medicine and other expanding applications of peptide amphiphiles.

AUTHOR INFORMATION

Corresponding Author

*Phone: +81-33296-5974. Fax: +81-33296-3184. E-mail: shimada.td@om.asahi-kasei.co.jp.

ACKNOWLEDGMENT

Part of this work was conducted under the trial-use program for neutron industrial applications funded by the Ministry of Education, Culture, Sports, Science and Technology. The authors thank Dr. Keishin Ishikawa of JAEA for his scientific and technical support. T.S. is very grateful to Prof. Kazuyuki Kuroda in Waseda University for fruitful discussion. M.T. would like to acknowledge financial support from the Armed Forces Institute for Regenerative Medicine, Enabling Technologies Program.

REFERENCES

(1) Israelachvili, J. N.; Mitchell, D. J.; Ninham, B. W. *J. Chem. Soc., Faraday Trans. 2* **1976**, *72*, 1525–1568.
(2) Kokkoli, E.; Mardilovich, A.; Wedekind, A.; Rexeisen, E. L.; Garg, A.; Craig, J. A. *Soft Matter* **2006**, *2*, 1015–1024.
(3) Cui, H.; Webber, M. J.; Stupp, S. I. *Peptide Sci.* **2010**, *94*, 1–18.
(4) Hamley, W. *Soft Matter* **2011**, *7*, 4122–4138.
(5) Hartgerink, J. D.; Beniash, E.; Stupp, S. I. *Science* **2001**, *294*, 1684–1688.
(6) Hartgerink, J. D.; Beniash, E.; Stupp, S. I. *Proc. Natl. Acad. Sci. U.S.A.* **2002**, *99*, 5133–5138.
(7) Silva, G. A.; Czeisler, C.; Niece, K. L.; Beniash, E.; Harrington, D. A.; Kessler, J. A.; Stupp, S. I. *Science* **2004**, *303*, 1352–1355.
(8) Beniash, E.; Hartgerink, J. D.; Storrie, H.; Stendahl, J. C.; Stupp, S. I. *Acta Biomater.* **2005**, *1*, 387–397.
(9) Zhang, S. *Nat. Biotechnol.* **2003**, *21*, 1171–1178.
(10) Stevens, M. M.; George, J. H. *Science* **2005**, *310*, 1135–1138.
(11) Behanna, H. A.; Donners, J. J. J. M.; Gordon, A. C.; Stupp, S. I. *J. Am. Chem. Soc.* **2005**, *127*, 1193–1200.
(12) Paramonov, S. E.; Jun, H.-W.; Hartgerink, J. D. *Biomacromolecules* **2006**, *7*, 24–26.
(13) Stendahl, J. C.; Rao, M. S.; Guler, M. O.; Stupp, S. I. *Adv. Funct. Mater.* **2006**, *16*, 499–508.
(14) Paramonov, S. E.; Jun, H.-W.; Hartgerink, J. D. *J. Am. Chem. Soc.* **2006**, *128*, 7291–7298.
(15) Shimada, T.; Lee, S.; Bates, F.; Hotta, A.; Tirrell, M. *J. Phys. Chem. B* **2009**, *113*, 13711–13714.
(16) Berndt, P.; Fields, G. B.; Tirrell, M. *J. Am. Chem. Soc.* **1995**, *117*, 9515–9522.
(17) Marqusee, S.; Robbins, V. H.; Baldwin, R. L. *Proc. Natl. Acad. Sci. U.S.A.* **1989**, *86*, 5286–5290.
(18) Koizumi, S.; Iwase, H.; Suzuki, J.-I.; Oku, T.; Motokawa, R.; Sasao, H.; Tanaka, H.; Yamaguchi, D.; Shimizu, H. M.; Hashimoto, T. *Physica B* **2006**, *385−386*, 1000–1006.
(19) Koizumi, S.; Iwase, H.; Suzuki, J.-I.; Oku, T.; Motokawa, R.; Sasao, H.; Tanaka, H.; Yamaguchi, D.; Shimizu, H. M.; Hashimoto, T. *J. Appl. Crystallogr.* **2007**, *40*, 474–479.
(20) Koizumi, S. *Focusing USANS Instrument Neutrons in Soft Matter*; John Wiley & Sons, Inc.: Hoboken, NJ, 2011; Chapter II.1.3.2.
(21) Roe, R. J. *Methods of X-ray and Neutron Scattering in Polymer Science*; Oxford University Press: Oxford, NY, 2000.